NJC

ROYAL SOCIETY OF CHEMISTRY

PAPER

View Article Online
View Journal

Cite this: DOI: 10.1039/c9nj04335g

The influence of support composition on the activity of Cu:Ce catalysts for selective catalytic reduction of NO by CO in the presence of excess oxygen†

Zahra Gholami, *[ab] Guohua Luo [a] and Fatemeh Gholami [c]

The catalytic activity of a series of Cu1:Ce3 catalysts supported on different supports (CNTs, AC, TiO_2, γ-Al_2O_3, and SiC) was studied for NO reduction by CO in the presence of excess oxygen. The effects of the support on the physicochemical properties of the Cu1:Ce3 catalysts were characterized by using SEM, TEM, N_2 adsorption–desorption, FTIR spectroscopy, XRD, XPS, CO-TPD, and NO-TPD techniques. The highest activity in the presence of oxygen was observed for the Cu1:Ce3/Al_2O_3 catalyst, and the NO conversion of 71.8% was obtained at 420 °C in the presence of 5% oxygen. The catalytic activity of the catalysts was significantly related to the synergistic interactions between surface oxygen vacancies and Cu^+ species in the catalysts, as well as the electron transfer and metal/support interface. The high activity of the Al_2O_3 supported catalyst in the presence of oxygen is attributed to the presence of catalytically active centers on the support as well as on the surface of the supported crystallites. The NO conversion slightly increased after increasing the O_2 concentration from 2% to 5%, due to the adsorption of more O_2 on the surface, thus providing more adsorbed O, which reacted with adsorbed CO to form CO_2 and provide oxygen vacancy for NO adsorption and dissociation. The adsorbed O can react with NO and form NO_2, which quickly reacts with CO to form N_2 and CO_2. A possible reaction mechanism was proposed for the reaction in the presence of excess oxygen.

Received 21st August 2019,
Accepted 27th November 2019

DOI: 10.1039/c9nj04335g

rsc.li/njc

1. Introduction

Nitrogen oxides (NO_x), which are generated by combustion processes from both mobile and stationary sources, are considered as the main atmospheric pollutants[1] and cause of environmental issues such as acid rain, ozone depletion, low visibility and fine particulates, and photochemical smog.[2,3] Selective catalytic reduction (SCR) is known as an efficient technique for NO_x reduction to harmless N_2.[4] Due to the co-existence of CO and NO in most of the exhaust gases, the reduction of NO by CO as a reducing agent (CO-SCR) has attracted more attention in recent decades.[2,5–7] Noble metal catalysts as efficient catalysts for CO-SCR have been widely used; however, due to the unavailability and high cost of these metals, their practical application is limited. Therefore, development of efficient non-precious and transition metal catalysts has attracted more attention.

Copper catalysts were found to be promising catalysts for NO reduction.[8,9] Owing to its excellent redox properties, oxygen storage/release capacity, and rich surface oxygen vacancy (SOV), the addition of cerium oxide can significantly enhance the catalytic activity.[3,10,11] Dispersion of the active metals on the support can enhance the catalytic activity by affecting the interaction between CO and NO. Copper-based catalysts can be supported on different carriers such as alumina,[12] zirconia,[13] TiO_2[8] and mesoporous silica.[14] Carbon-based materials can also be used as supports for NO_x reduction by CO at low temperature (below 300 °C).[15] Yao *et al.*[16] used $Ce_{0.67}Sn_{0.33}O_2$, $Ce_{0.67}Zr_{0.33}O_2$, and $Ce_{0.67}Ti_{0.33}O_2$ as supports for the preparation of copper-based catalysts for the NO + CO reaction. They found that CuO/$Ce_{0.67}Zr_{0.33}O_2$ was reduced more easily than other catalysts, most probably due to the differences in the electronegativity of the dopant. The more significant gradient of electronegativity between Cu and M (M = Ce, Zr, and Ti) was reported to be beneficial for obtaining Cu^+/Cu^0 species. It was also revealed that because of the shifting of redox equilibrium (Cu^{2+} + Ce^{3+} ↔ Cu^+ + Ce^{4+}) to the right, Cu^+ exists in the catalyst at ambient temperature.

[a] Beijing Key Laboratory of Green Chemical Reaction Engineering and Technology, Department of Chemical Engineering, Tsinghua University, Beijing 100084, China
[b] Unipetrol Centre of Research and Education, a.s, Areál Chempark 2838, Záluží 1, 436 70 Litvínov, Czech Republic. E-mail: Zahra.Gholami@unicre.cz; Tel: +420 471 122 239
[c] New Technologies – Research Centre, University of West Bohemia, Engineering of Special Materials, Plzeň 301 00, Czech Republic

† Electronic supplementary information (ESI) available. See DOI: 10.1039/c9nj04335g

Compared with mobile exhaust gas, flue gas from stationary sources, such as coal-fired power plants, contains much more oxygen. Excess amounts of O_2 may also lead to CO consumption (reducing agent for NO reduction) and result in high CO oxidation, and also cause the deactivation of active sites by oxidizing the active metals. The catalytic performance of Fe/Co catalyst over activated semicoke (ASC) for NO reduction by CO was investigated.[7,15] The catalyst revealed excellent performance under oxygen-free conditions, but due to the oxidation of active metal sites in the presence of oxygen, the NO + CO reaction was strongly inhibited; CO will be quickly consumed, and oxygen preferentially oxidizes CO over the carbon support; then, NO–carbon reaction will be the main reaction. Formation of surface oxygen compounds in the presence of oxygen could enhance the NO–carbon reaction. The catalytic performance of Cu–Fe catalysts supported on γ-Al_2O_3 and CNTs for NO + CO reaction has been studied.[17] Results revealed that at 500 °C, the NO conversions of 100% and 80% were obtained over CNT and γ-Al_2O_3 supported catalysts, respectively. Catalytic activity was affected by the nature and properties of the support that influenced the metal dispersion and reduction properties.

Catalytic performance of a transition metal Cu/TiO_2 catalyst has been evaluated for the NO + CO reaction at 500 °C and a GHSV of 75 000 h^{-1}, and this catalyst shows a NO conversion of 60% with a good stability in the presence of oxygen.[18] Catalytic performance of a Cu:Ce/CNT catalyst for the reduction of NO_x by CO at 220 °C has been studied by our research group,[19] and the highest conversion of NO_x (96%) was obtained at 220 °C, at $O_2/CO \leq 0.6$. Shifting of the redox equilibrium to the right resulted in the formation of more Cu^+. However, in the presence of excess oxygen ($O_2/CO \geq 0.6$), the NO + CO reaction did not occur, and the catalyst can effectively catalyze the CO oxidation reaction.

In the present study, we prepared a series of Cu1:Ce3 catalysts supported on different carriers with different physico-chemical properties and different metal–support interactions, to investigate the effect of support on the catalytic activity for reduction of NO by CO in the presence of excess oxygen. The catalysts were characterized by X-ray diffraction (XRD), X-ray photoelectron spectroscopy (XPS), N_2 adsorption–desorption, temperature-programmed desorption (CO-TPD and NO-TPD), field-emission scanning electron microscopy (FESEM), and transmission electron microscopy (TEM). We believe that this work will provide an in-depth understanding of the effect of the nature and properties of the supports in the CO-SCR reaction for NO_x reduction.

2. Experimental section

2.1. Pretreatment of AC and CNTs

Coconut shell activated charcoal with a specific surface area of 600–800 $m^2\ g^{-1}$ and a size of 50–200 mesh was selected as a substrate, and it was treated with hydrochloric acid (AR, Beijing Chemical Works) according to the method provided in our previous study.[19] Surface modification and oxidation of the MWCNTs (CNano Technology Ltd, China, 95% < purity < 97%) were performed using an acid mixture of HNO_3 (65%, Beijing Modern Oriental Fine Chemicals Co., Ltd) and H_2SO_4 (98%, Modern Oriental (Beijing) Technology Development Co., Ltd), with a $HNO_3 : H_2SO_4$ ratio of 3 : 1 (v/v), according to our previous research work.[19] γ-Al_2O_3 (98%, Modern Oriental (Beijing) Technology Development Co., Ltd, >99%), TiO_2 nanopowder with the particle size of 21 nm (ALDRICH Chemistry, 99.5%), and SiC (ALDRICH Chemistry, 99.5%) were used without any pretreatment.

2.2. Synthesis of supported catalysts

The Cu1:Ce3 catalysts (Cu : Ce (molar ratio) = 1 : 3) with 20 wt% total metal loading were prepared by a co-impregnation method. First, the required amounts of precursors $Cu(NO_3)_2{\cdot}3H_2O$ (>99%, Beijing Modern Eastern Fine Chemicals Co., Ltd, China) and $Ce(NO_3)_3{\cdot}6H_2O$ (>99%, Modern Oriental (Beijing) Technology Development Co., Ltd, China) were dissolved in deionized water. Then, this aqueous solution was added dropwise to the supports at room temperature and under continuous stirring. The mixtures were subjected to ultrasonic treatment for 180 min, followed by stirring for 24 h, at room temperature. Afterward, the samples were dried at 120 °C overnight and calcined at 350 °C in an Ar atmosphere for 3 h. All supported catalysts were prepared using the same procedure.

2.3. Catalyst characterization

The catalysts were characterized in terms of surface properties and morphology, surface area, porosity, phase, particle size, and reducibility properties. The morphology of the prepared catalysts was studied by using scanning electron microscopy (JSE-6700F) and transmission electron microscopy (TEM, JEM-2100). The phase structures of the catalysts were analyzed using X-ray diffraction (XRD, D8 ADVANCE Rigaku D/max-RB) with Cu Kα radiation (k = 1.5408 Å) at 60 kV and 80 mA. The surface properties were measured by using nitrogen adsorption/desorption at liquid nitrogen temperature using a QuadraSorb SI system. Before measurements, the sample was degassed at 150 °C. The active surface functional groups and surface chemistry of the synthesized catalysts were determined using a Thermo Scientific Nicolet (NEXUS 670 FTIR) spectrometer. A Thermo Scientific K-alpha photoelectron spectrometer was used for performing X-ray photoelectron spectroscopy (XPS). The temperature programmed desorption (TPD) of NO, and CO analysis were performed in a flow reactor equipped with a thermal conductivity detector (TCD) according to the method described in our previous study.[19]

2.4. Catalytic activity evaluation

The catalytic activity for the reduction of NO by CO was tested in a fixed bed tubular reactor with a vertical furnace mounted inside (Fig. S1, ESI†). Catalytic activity testing was performed using 200 mg of catalyst at 220 °C. The reaction temperature was measured by a thermocouple located above the catalyst bed inside the reactor. Before starting the reaction, the catalyst was flushed *in situ* with helium at 200 °C for 60 min. The temperature of the reactor was adjusted to the required temperature, and then

the reactant gases were introduced to the reactor. The feed gas contained 250 ppm NO, 5000 ppm CO, 2% and 5% (vol) O_2, and He as the balance gas. The total flow rate of the feed gas was 300 mL min^{-1}. A chemical luminescence $NO/NO_2/NO_x$ analyzer (CAI-600 HCLD) was used for the analysis of the NO_x compounds, and the concentrations of O_2, CO, and CO_2 were analyzed using a PG810 multi-gas detector.

3. Results and discussion

3.1. Characterization of catalysts

Fig. 1 shows the morphologies of the supported Cu1:Ce3 catalysts. The FESEM images show aggregates of fine particles. An evident agglomeration of particles in SiC and TiO_2 supported catalysts was observed. In the AC supported catalyst, particle agglomeration and an uneven distribution of the particles were also observed. Cu1:Ce3/γ-Al_2O_3 showed a better and more homogenous dispersion of metals on the surface of the catalyst. Good dispersion of metals can also be seen in the elemental mapping analysis of the catalysts (Fig. S2, ESI†). The transmission electron microscope images of the catalysts are shown in Fig. 2. TEM images and elemental mapping confirmed the good dispersion of metals for all prepared catalysts. The particle sizes were between 3–5 nm for the Cu1:Ce3 catalysts, and it can be seen that the metal particles were dispersed uniformly on AC and γ-Al_2O_3 supported catalysts, while for other samples (TiO_2, SiC, and CNT supported catalysts), some agglomeration can be seen.

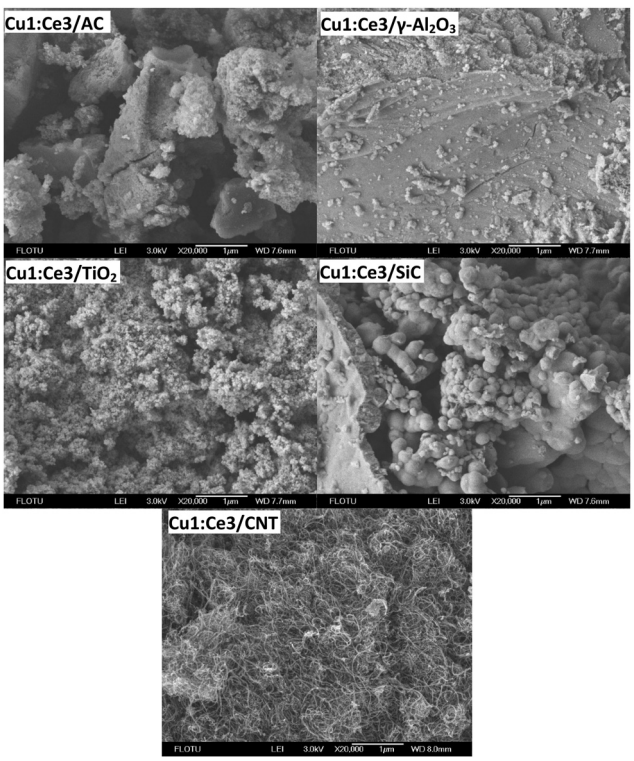

Fig. 1 FESEM images of different Cu1:Ce3 catalysts supported on different solid carriers.

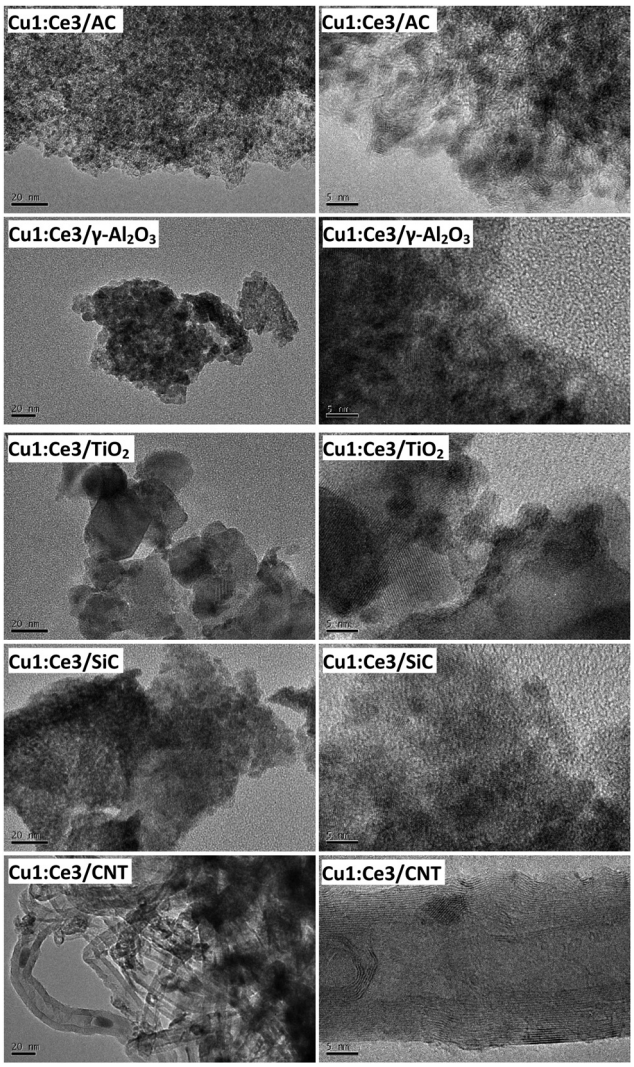

Fig. 2 TEM images of different Cu1:Ce3 catalysts supported on different solid carriers.

Fig. 3 shows the XRD patterns of Cu1:Ce3 supported on AC, γ-Al_2O_3, TiO_2, SiC, and CNTs. The location of the peaks confirms that Cu and Ce were properly loaded on the surface of

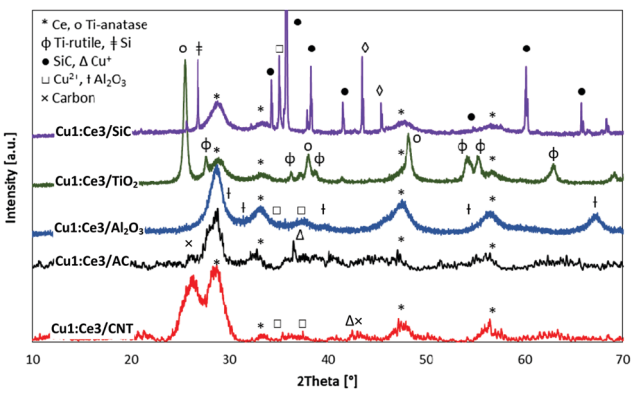

Fig. 3 XRD patterns of different Cu1:Ce3 catalysts supported on different solid carriers.

each support. In addition to the peaks belonging to Cu and Ce, peaks for amorphous carbon, and γ-Al_2O_3,[20] TiO_2[21] and SiC[22,23] were detected. The TiO_2 support was present in both rutile and anatase phases.[21] The peak at a 2θ value of $\sim 25^\circ$ corresponds to the graphite plane (002) reflection, which is evident for CNT, AC and SiC supported catalysts in this research.[24]

XRD patterns revealed that the peaks at 2θ = 28.5°, 33.1°, 47.5°, and 56.8° correspond to the cubic fluorite structure of ceria.[19,25] The diffraction lines corresponding to (111), (200), (220), (311) of the CeO_2 phase (JCPDS No. 34-0394) were detected for all samples, which slightly shifted to lower degrees due to the interaction with Cu and the support and replacement of Ce^{4+} by larger sized Ce^{3+}.[26,27] It can be seen that the intensity of these peaks for carbonaceous supported catalysts is more obvious, which could be due to the weaker interaction between the metal and supports in these catalysts. There are not very visible peaks for copper oxide crystal phases in all XRD patterns, which could be due to the incorporation of copper into the ceria lattice.[25,28,29] However, it has also been reported that deposits with such a small copper grain size yield no X-ray diffraction pattern.[30,31]

The surface properties of the different Cu1:Ce3 catalysts are shown in Table 1. The pore volume of the Cu1:Ce3/CNT catalyst was found to be 0.92 cc g^{-1}, and that of the AC, Al_2O_3, and TiO_2 supported catalysts was 0.17 cc g^{-1}, 0.27 cc g^{-1}, and 0.24 cc g^{-1}, respectively. The pore volume for the SiC supported catalyst was significantly smaller than the pore volume for the other catalysts, and thus the porosity was correspondingly smaller as well. The corresponding pore sizes of the prepared catalysts were determined using the Barrett–Joyner–Halenda (BJH) method (for the mesopore range) and the density functional theory (DFT) method for the AC supported catalyst with a microporous structure. It was observed that the pore sizes of the CNT, Al_2O_3, TiO_2 and SiC supported catalysts were 3–17 nm, in the mesoporous range. The Cu1:Ce3/CNT catalyst shows the highest pore size of 16.77 nm and AC has the lowest pore size of 1.23 nm. The surface area of the CNT and AC supported catalysts is 157.2 m^2 g^{-1} and 176.4 m^2 g^{-1}, respectively. The surface area of the Cu1:Ce3/SiC catalyst (8.62 m^2 g^{-1}) was considerably lower than those of the other catalysts. The very low surface area and pore volume of the SiC supported catalyst were expected to have a noticeable effect on the catalytic performance of this catalyst. The adsorption–desorption isotherms of the catalysts are shown in Fig. S3 (ESI†). The nitrogen adsorption of the catalysts can be expressed as type IV, with a H4 hysteresis loop for the AC supported catalyst (Cu1:Ce3/AC) and a H3 hysteresis loop for the other catalysts (Cu1:Ce3/CNT, Cu1:Ce3/Al_2O_3, Cu1:Ce3/TiO_2 and Cu1:Ce3/SiC).[32,33] A characteristic feature of this type of isotherm is its hysteresis loop, which is associated with capillary condensation taking place in mesopores, and a limited uptake over the range of high P/P_0. The initial part of the type IV isotherm is attributed to monolayer–multilayer adsorption. Many mesoporous materials give type IV isotherms. The type H4 hysteresis loop indicated the existence of pores with narrow slit-like geometry, generally observed with complex materials containing both micropores and mesopores. This type of isotherm (H4) is usually given by many activated carbons and some other nanoporous materials. The type H3 hysteresis loop is typically observed with the accumulation of plate-like and nano-sized particles having slit-shaped pores.[32,33]

The FTIR spectra of Cu1:Ce3 catalysts are shown in Fig. 4. The peak at around 650–700 cm^{-1} in the FTIR spectrum of the catalysts is ascribed to the stretching of the metal–oxygen bonds of Cu–O and Ce–O.[34] The broad peaks at 1100 cm^{-1} in the Cu1:Ce3/TiO_2 spectrum are attributed to the characteristic

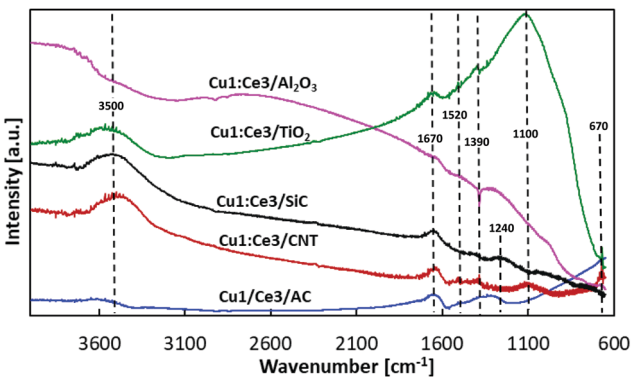

Fig. 4 FTIR spectra of different Cu1:Ce3 catalysts supported on different solid carriers.

Table 1 XPS data of the synthesized catalysts, pore diameter, pore volume, surface area and porosity of Cu1:Ce3 catalysts supported on different solid carriers

	Catalysts				
	Cu1:Ce3/CNT	Cu1:Ce3/AC	Cu1:Ce3/Al_2O_3	Cu1:Ce3/TiO_2	Cu1:Ce3/SiC
Cu (at%)	0.9	0.95	0.86	1.44	0.87
Ce (at%)	1.97	1.87	1.89	2.60	2.2
O (at%)	7.83	9.75	28.15	27.98	28.2
C (at%)	89.3	87.42	8.43	14.98	13.76
Cu^+/Cu^{2+} [a]	4.01	2.65	1.29	1.59	0.4
Ce^{3+}/Ce^{4+} [b]	0.55	0.88	0.56	0.68	0.57
Surface area (m^2 g^{-1})	157.25	176.36	84.87	50.78	8.62
Pore volume (cc g^{-1})	0.92	0.27	0.17	0.24	0.04
Pore size (nm)	16.77[c]	1.23[d]	3.80[c]	12.09[c]	3.32[c]

[a] Area ratio of Cu^+/Cu^{2+} estimated by considering the deconvoluted peak areas of Cu^+ and Cu^{2+}. [b] Area ratio of Ce^{3+}/Ce^4 estimated by considering the deconvoluted peak areas of Ce^{3+} and Ce^{4+}; Ce^{3+}/Ce^4 = area (Ce^{3+})/area (Ce^{4+}) = area ($v^0 + v' + u^0 + u'$)/area ($v + v'' + v''' + u + u'' + u'''$). [c] Calculated based on BJH method. [d] Calculated based on DFT method.

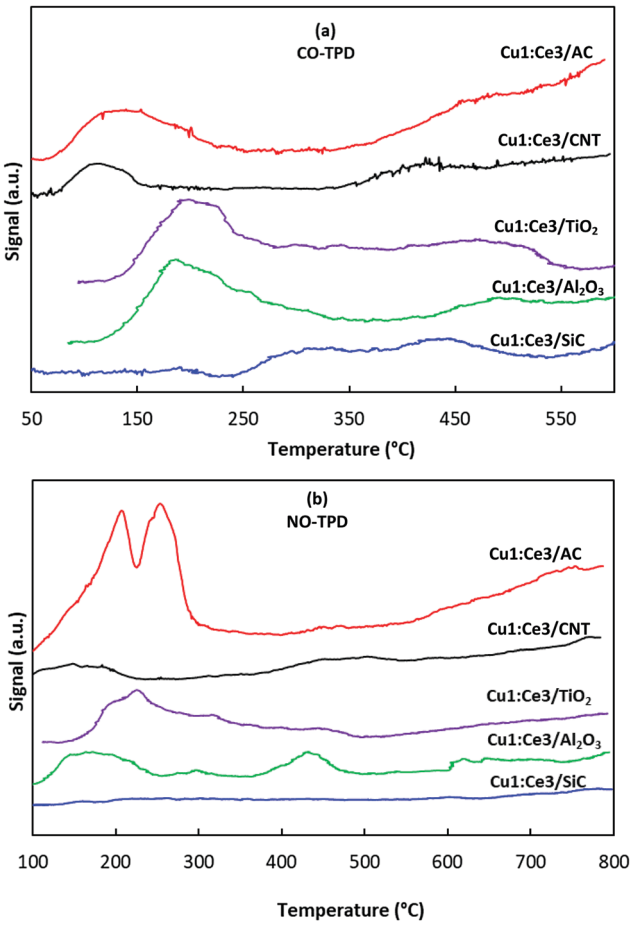

Fig. 5 (a) CO-TPD profiles, and (b) NO-TPD profiles of Cu1:Ce3 catalysts supported on different solid carriers.

vibration of Ti–O.[35] The asymmetric vibration modes of the Si–O–Si bonds[36] and Si–C stretching vibration[37] could be seen at 1070 cm^{-1} and 1260 cm^{-1} in the FTIR spectrum of the Cu1:Ce3/SiC catalyst. The peak between 1500 and 1700 cm^{-1} corresponded to different carbonate groups, *i.e.*, C═O, C═C.[38] The peak at 1310–1390 cm^{-1} and the broad band in the range from 3400 cm^{-1} to 3700 cm^{-1} belong to the stretching vibration of O–H bonds.[39]

The CO-TPD and NO-TPD characterization results of the catalysts are shown in Fig. 5. From Fig. 5(a), it can be seen that the CNT and AC supported catalysts had a peak at a temperature around 110–150 °C, while the peak for Al_2O_3 and TiO_2 was observed at a higher temperature of 180–230 °C. The catalytic activity is expected to be decreased upon shifting the peak positions to a higher temperature. The low-temperature peak of the catalysts can be assigned to the weakly adsorbed CO species on the Cu^0 and/or Cu^+ sites on the catalyst surface.[19] The presence of more Cu^+ on the surface of the catalyst could increase the CO adsorption at the surface, which can be confirmed by XPS analysis of the catalysts. The peak for the Al_2O_3 and TiO_2 catalysts shifted to a higher temperature, which could be due to the strong adsorption of CO by active metals in these catalysts, which leads to increasing the desorption temperature. This increase in the CO desorption temperature could also be due to the lower electronic transfer between the metals, as well as the electron transfer between the metals and the supports. Better electron transfer leads to the shifting of redox equilibrium ($Cu^{2+} + Ce^{3+} \leftrightarrow Cu^{+} + Ce^{4+}$) to the right and the formation of more Cu^+, which facilitate the adsorption of CO molecules at the surface of the catalyst.

The NO-TPD profiles of the catalysts are shown in Fig. 5(b). The shape of the desorption pattern and the amount of adsorbed NO were affected by the composition of the catalyst and type of support. NO desorption peaks were observed at around 100–300 °C and 400–800 °C, indicating that NO was adsorbed on different active sites. The peaks below 150 °C can be ascribed to the physisorbed NO and the decomposition of monodentate nitrate species and bridged nitrite, while the peaks at higher temperature belong to the decomposition of bridged nitrate and bidentate nitrate species, which exhibit high thermal stability.[40,41]

It can be seen that the NO desorption from the CNT supported catalyst is lower than those of the others, which confirms the higher affinity of AC, Al_2O_3, and TiO_2 supported catalysts for the adsorption of NO species at low temperature. The N–O bond can be weakened and dissociated by back-donation and the release of unpaired electrons into the empty orbitals of the adsorbed NO species.[42] The AC supported catalyst, with a large surface area and the presence of different organic groups, shows two sharp peaks for NO desorption at temperatures below 300 °C. It is worth mentioning that not only both the small size of the activated carbon pore and the specific surface area have important influences on gas adsorption, but also the surfaces of the polar groups have obvious influences on gas adsorption.[43,44] Oxygen containing functionalities are generated when the carbon surface is oxidized. Several oxygen containing functionalities (acidic, basic and neutral) were detected on the surface of activated carbon, such as carboxylic, phenol, carbonyl, pyrone, quinone, ether groups, *etc.*[43] Both CO and NO are polar molecules; however, due to its very small dipole moment (0.112 D), CO is usually considered to be almost nonpolar.[44] Therefore, more NO molecules could adsorb on the surface of the AC supported catalyst than on other catalysts. The reaction of initially adsorbed CO with the lattice oxygen could provide oxygen vacancies for NO adsorption, while the higher adsorption of NO at low temperature could reduce the chance for initial adsorption of O_2 and CO on the surface of the catalyst. However, the reaction rate for NO oxidation was very low, which resulted in low NO conversion.

XPS analysis was used to evaluate the elemental oxidation and surface composition of the catalysts. Fig. 6 shows the XPS spectra of Cu 2p of the prepared catalysts. The peaks at 932.5 and 951.5 eV can be assigned to Cu $2p_{3/2}$ and $2p_{1/2}$ of Cu_2O, respectively. The peaks at 934.5 and 954.5 eV that can be assigned to the Cu $2p_{3/2}$ and Cu $2p_{1/2}$ peaks also confirm the formation of CuO and the shake-up or satellite peak is also located at 938.6–948.6 eV.[45,46] The content of Cu^+/Cu^{2+} of the catalysts (Table 1) was found to be in the following order: Cu1:Ce3/CNT (4.01) > Cu1:Ce3/AC (2.65) > Cu1:Ce3/TiO_2 (1.59) > Cu1:Ce3/Al_2O_3 (1.29) > Cu1:Ce3/SiC (0.4). The presence of Cu^+ and Ce^{3+}

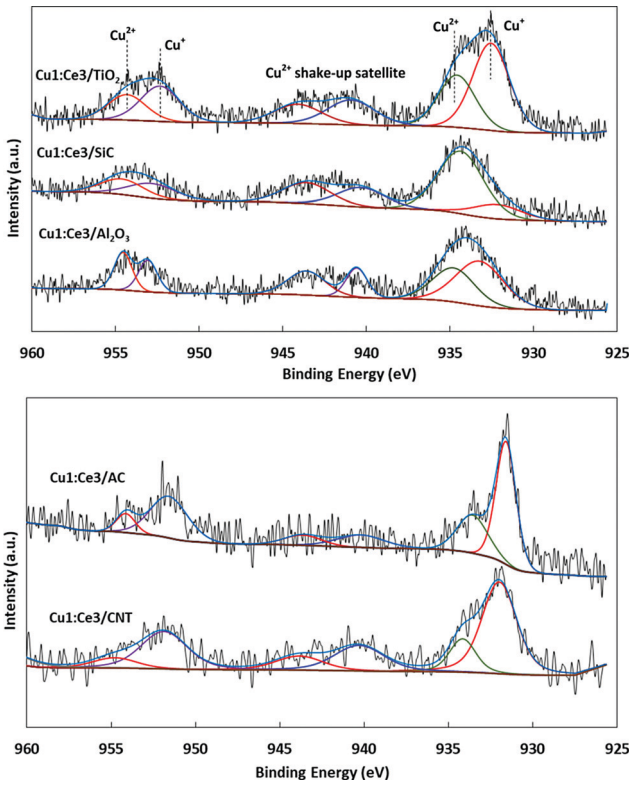

Fig. 6 XPS spectra of Cu 2p of Cu1:Ce3 catalysts supported on different solid carriers.

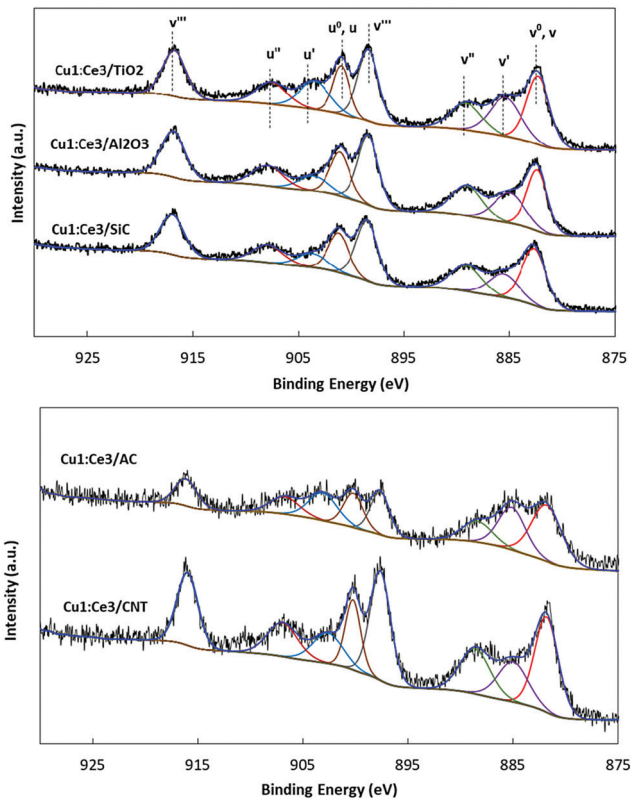

Fig. 7 XPS spectra of Ce 3d of Cu1:Ce3 catalysts supported on different solid carriers.

species indicates that the redox equilibrium is shifting to the right, which has an important effect on the catalytic activity.[46,47]

The Ce^{3+}/Ce^{4+} contents of the catalysts were calculated to be 0.55, 0.88, 0.56, 0.68, and 0.57 for Cu1:Ce3/CNT, Cu1:Ce3/AC, $Cu1:Ce3/Al_2O_3$, $Cu1:Ce3/TiO_2$, and Cu1:Ce3/SiC, respectively. The ratio of Cu^+/Cu^{2+} was positively correlated with the ratio of Ce^{3+}/Ce^{4+} and the catalyst with low Cu^+/Cu^{2+} also has low Ce^{3+}/Ce^{4+}, which could be due to the strong interaction of active metal and the supports, which leads to the lower electron transfer between the metals and also between metal and support. However, the CNT supported catalyst with the highest Cu^+/Cu^{2+} shows a low Ce^{3+}/Ce^{4+}. The formation of more Cu^+ could be due to the higher electronegativity of Cu (1.9) than that of Ce (1.1), which increases the tendency to capture electrons of Cu.[19] Thus, Cu^{2+} can accept electrons to create more Cu^+ and Cu^0. Moreover, CNTs act as both electron donors and acceptors,[48] thus they can enhance the electron transfer from support to Cu^{2+} to form more Ce^+, and at the same time, they can also increase the transfer of electron from Ce^{3+} to the support to form more Ce^{4+} and decrease the Ce^{3+}/Ce^{4+} ratio.

It is expected that the catalyst with a high Cu^+/Cu^{2+} shows higher activity for NO reduction reaction.[45,46] Therefore, the highest catalytic activity is anticipated for the CNT supported catalyst, and the SiC supported catalyst is expected to have the lowest activity. The electron transfer and metal/support interface are essential parameters in the catalytic performance. The electron transfer could be available also between metal and support. However, compared to the electron transfer in the redox equilibrium between Cu and Ce, the rate of the electron transfer between metal and support might be lower.[47,49] Besides, the higher Cu^+ content leads to a higher tendency for CO adsorption, which increases the number of oxygen vacancies on the surface of the catalyst.[50,51]

Fig. 7 shows the Ce 3d spectra of the catalysts supported on different solid carriers. The peak bands labeled (u, v), (u″, v″), and (u‴, v‴) represent the $3d^{10}4f^0$ state corresponding to Ce^{4+} ions, and the peaks labeled (v^0, u^0) and (u′, v′) represent the $3d^{10}4f^1$ initial electronic state corresponding to Ce^{3+} ions.[45,46] This behavior has also been confirmed by the shifting of the desorption peaks in CO-TPD analysis. However, during the NO reduction by CO in the presence of oxygen, it can also enhance the possibility of CO oxidation reaction instead of NO + CO reaction and reduce the NO conversion.

The O 1s XPS spectra of Cu1:Ce3 catalysts are shown in Fig. 8. The first peak at 528.6 eV corresponds to the lattice oxygen bonding of CeO_2, and the O 1s peaks of CuO and Cu_2O were observed at 529.5 and 530.5 eV, respectively.[52] The oxygen bonds belonging to Cu_2O are considerably higher in number in the CNT and AC supported catalysts. This could be due to the enhanced electron transfer between the carbonaceous supports, which leads to the shifting of redox equilibrium to the right and formation of more Cu^+ on the surface of catalysts. Moreover, it can be seen that for the Al_2O_3, TiO_2 and SiC supported catalysts, the peak belonging to CeO_2 is not very obvious, which also indicated the low electron transfer between the metals as well as the metals and the supports.

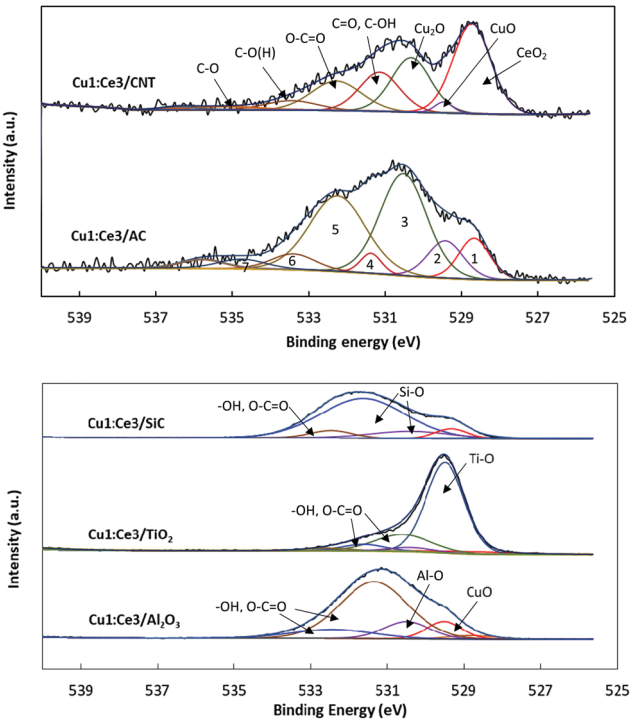

Fig. 8 XPS spectra of O 1s for Cu1:Ce3 catalysts supported on different solid carriers.

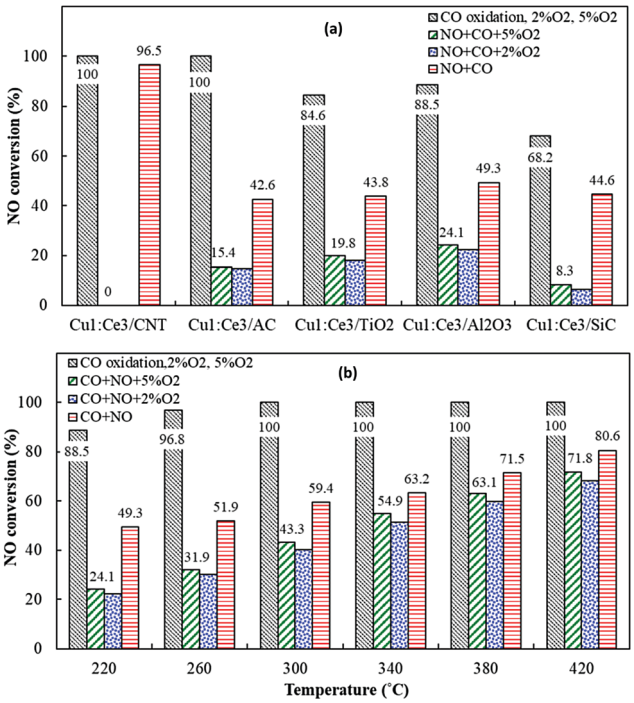

Fig. 9 (a) Effect of support on NO–CO reaction over Cu1:Ce3 catalysts; reaction conditions: NO = 250 ppm, CO = 5000 ppm, and total flow rate: 300 ml min^{-1}; catalyst: 200 mg, and temperature: 220 °C; (b) effect of temperature on catalytic activity of Cu1:Ce3/Al_2O_3 catalyst.

Due to the presence of numerous functional groups in CNT and AC, several peaks can be observed in the O 1s spectra of these catalysts. The peaks belonging to carbonyl and carboxylic acids (C═O) were observed at 531.4 eV. The peak at 532.5 eV was assigned to the O═C–O of lactone, ester and carboxylic groups. The C–O bonds of ether and hydroxyl groups were observed at 533.4 and 534.8 eV.[53,54]

The peaks belonging to the lattice oxygen and the hydroxyl oxygen can be seen in the O 1s spectrum of TiO_2 supported catalysts, at 529.5 and 531.1 eV, respectively,[55,56] and the small peak at 532.7 eV belongs to the hydroxide O–H groups on the surface of the catalyst.[57] The peak belonging to the oxygen in Al_2O_3 (Al–O) is located at 530.6 eV, while peaks at 531.3 and 532.4 eV are ascribed to the O in H_2O, and OH^- bonds in aluminum hydroxide (AlOOH), respectively.[58–60] The peaks at 530.2 and 532.5 eV in the SiC supported catalyst are attributed to the low-coordinated and high coordinated O–Si, respectively, while the peak located at 531.6 eV belongs to the O–Si–C bond.[61–63] It was found that the main type of functional group for the Cu1:Ce3/CNT and Cu1:Ce3/AC catalysts was O═C–O. Existence of abundant surface oxygen groups in AC leads to the decreased hydrophobicity of carbon, ion-exchange capability, and electronic properties.[19] These oxygen-containing functional groups could affect the interaction between the metals and the supports and dispersion of the metals on the supports.

3.2. Catalytic performance tests

The catalytic activity of Cu1:Ce3 catalysts supported on different solid carriers in the NO–CO reaction and effect of oxygen on their performance have been evaluated. NO_x conversion without O_2 over the CNT-supported (96%) catalyst was higher than the conversion over Cu1:Ce3 catalysts supported on other supports (Fig. 9). It is noticeable that due to the quick reaction of NO_2 with CO to form N_2 and CO_2, formation of NO_2 was very low (~1%) for all the reactions over all the different catalysts, and so it has not been shown in the graphs. The CNTs, with high electron transfer capability and conductivity, enhanced the formation of more Cu^+ on the surface of the catalysts (confirmed by XPS analysis), which also shows a high tendency for CO adsorption. Owing to the competition between NO and oxygen for CO, the NO + CO reaction is a non-selective reduction reaction in the presence of oxygen. At increased oxygen concentrations, CO preferentially reacts with oxygen. As has been mentioned before, over the carbonaceous supported catalysts, the presence of abundant surface oxygen groups resulted in a decrease in hydrophobicity, ion-exchange capability, and electronic properties.[19] The interaction between the metals and the supports and also dispersion of the active metals on the surfaces could be affected by these oxygen-containing functional groups. Over the metal oxide supported catalysts (TiO_2, Al_2O_3, and SiC), the affinity to initial adsorption of CO on active sites of the catalyst decreased, and at the same time, the strong interaction of the active metals and supports leads to the lower activity.

CO oxidation reaction ($CO + 1/2O_2 \rightarrow CO_2$) is the most plausible reaction in the presence of oxygen. Over the carbonaceous supported catalysts, CO or CO_2 could also be produced from the oxidation of carbon on the surface of the catalysts ($C + 1/2O_2 \rightarrow CO$, $C + O_2 \rightarrow CO_2$). In the presence of 2% and 5% oxygen, at 220 °C, the CO oxidation reached 100%, and the NO conversion significantly dropped to 0 and 15% for the CNT and

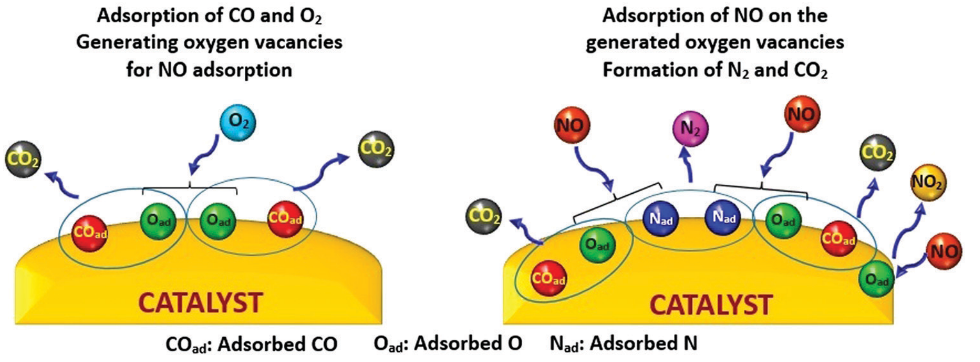

Fig. 10 Possible reaction mechanism for NO reduction by CO in the presence of O_2.

AC supported catalysts, respectively. CO oxidation over the Al_2O_3 supported catalyst was 88.5% and it increased to 100% upon increasing the temperature to 300 °C; the possibility of CO oxidation reaction is much higher than that of the NO + CO reactions ($NO + CO \rightarrow CO_2 + 1/2N_2$, $2NO + CO \rightarrow CO_2 + N_2O$).

In the presence of oxygen, the CNT supported catalyst, with the highest amount of Cu^+/Cu^{2+}, did not show any catalytic activity, while the NO conversion of 24% was observed for Cu1:Ce3/Al_2O_3; and by increasing the reaction temperature to 420 °C, the NO conversion increased to 72.8%. The NO conversion was slightly enhanced after increasing the O_2 concentration from 2% to 5%, which could be due to the adsorption of more O_2 on the surface and providing more O(ads), which can facilitate the formation of NO_2, which can rapidly react with CO to form N_2 and CO_2. It has been reported that the reduction of NO could be promoted by the addition of oxygen over copper catalysts supported on Al_2O_3.[64] A possible mechanism for the NO reduction by CO in the presence of oxygen was proposed (Fig. 10).

It is suggested that in the presence of oxygen, CO is adsorbed on the surface of the catalyst and creates an oxygen vacancy by reacting with lattice oxygen. NO is adsorbed on the generated oxygen vacancy, and the oxygen atom of the adsorbed NO creates a bond with the adjacent metallic atom. The N–O bond is weakened and divides to N and O adsorbed species. Two separated N atoms can produce N_2 or one N atom can react with another NO species to form N_2O. Meanwhile, new lattice oxygen is formed on the catalyst surface. In addition, an O_2 molecule was also adsorbed on the surface of the catalyst and produced two adsorbed O atoms, which are able to react with adsorbed CO and NO molecules and produce CO_2 and NO_2, and NO_2 subsequently reacted with CO to produce N_2 ($2NO_2 + 4CO \rightarrow 4CO_2 + N_2$).[65]

4. Conclusions

In this study, a series of Cu1:Ce3 catalysts supported on different solid carriers, *i.e.*, CNT, AC, Al_2O_3, TiO_2, and SiC, was prepared by the co-impregnation method to investigate the influence of the type and nature of the support on the properties of catalysts and catalytic performance in NO reduction by CO. In the absence of O_2, a high catalytic activity for the NO + CO reaction was observed over the Cu1:Ce3/CNT catalyst, due to the large concentration of SOV, superior reducing capability, high Cu^+ species content and also the synergistic effect between SOV and Cu^+ species in this catalyst. However, under the same reaction conditions, the other catalysts did not show good catalytic performance. Formation of Cu^+ on the surface of the CNT supported catalysts was boosted due to their high conductivity and electron transfer capability, while XPS results proved that the concentration of Cu^+ in AC, Al_2O_3, TiO_2, and SiC supported catalysts was lower than that of Cu1:Ce3/CNT. The active metal/support interface and electron transfer are essential parameters for the catalytic activity and a strong interaction between the metals and supports leads to a higher reduction temperature and a decrease in the amount of reduced metal on the surface of the catalyst, which is more prominent in the metal oxide supports (*i.e.*, Al_2O_3 and TiO_2). Over the non-carbonaceous supported catalysts, the affinity to adsorption of CO on active sites of the catalyst decreased, and at the same time, the strong interaction of the active metals and support leads to the lower catalytic activity. However, the larger surface area led to an increase in the area of interface between catalyst and reactant and increased the catalytic performance.

The highest activity in the presence of 5% oxygen was observed for the Cu1:Ce3/Al_2O_3 catalyst (NO conversion of 24.1% at 220 °C), which significantly increased to 71.8% upon increasing the reaction temperature to 420 °C. The NO conversion slightly increased after increasing the O_2 concentration from 2% to 5%. In the presence of excess oxygen, O_2 adsorbed on the surface of the catalyst and produced two adsorbed O atoms, which can react with CO and produce CO_2, and then NO adsorbed on the provided oxygen vacancy and dissociated to adsorbed N and O atoms. Two N species could combine to form N_2, and NO species could also react with adsorbed O atoms to produce NO_2, which then quickly reacts with CO.

Conflicts of interest

There are no conflicts to declare.

Acknowledgements

This work was supported by the Research Fellowship for International Young Scientists, National Natural Science Foundation of

China (NSFC) under Grant number 21750110436; Ministry of Education, Youth and Sports of the Czech Republic under the "National Sustainability Programme I" under Grant number LO1606; and Ministry of Education, Youth and Sports under the "National Sustainability Programme I", [reg. no. CZ.1.05/2.1.00/03.0088] under Grant number CENTEM PLUS (LO1402).

References

1 X. Dai, W. Jiang, W. Wang, X. Weng, Y. Shang, Y. Xue and Z. Wu, *Chin. J. Catal.*, 2018, **39**, 728–735.
2 K. Liu, Q. Yu, J. Liu, K. Wang, Z. Han, Y. Xuan and Q. Qin, *New J. Chem.*, 2017, **41**, 13993–13999.
3 Y. Bai, X. Bian and W. Wu, *Appl. Surf. Sci.*, 2019, **463**, 435–444.
4 X. Cheng, X. Zhang, M. Zhang, P. Sun, Z. Wang and C. Ma, *Chem. Eng. J.*, 2017, **307**, 24–40.
5 S. Wu, X. Li, X. Fang, Y. Sun, J. Sun, M. Zhou and S. Zang, *Chin. J. Catal.*, 2016, **37**, 2018–2024.
6 G. Caravaggio, L. Nossova and R. Burich, *Emiss. Control Sci. Technol.*, 2016, **2**, 10–19.
7 P. Sun, X. Cheng, Z. Wang, Y. Lai, C. Ma and J. Chang, *J. Energy Inst.*, 2019, **92**, 488–501.
8 N. Liu, X. Chen, J. Zhang and J. W. Schwank, *Catal. Today*, 2015, **258**(Part 1), 139–147.
9 N. Takagi, K. Ishimura, H. Miura, T. Shishido, R. Fukuda, M. Ehara and S. Sakaki, *ACS Omega*, 2019, **4**, 2596–2609.
10 R. Zhang, W. Y. Teoh, R. Amal, B. Chen and S. Kaliaguine, *J. Catal.*, 2010, **272**, 210–219.
11 K. Liu, Q. Yu, B. Wang, Z. Han, J. San and Q. Qin, *New J. Chem.*, 2019, **43**, 13571–13583.
12 L. Zhang, X. Yao, Y. Lu, C. Sun, C. Tang, F. Gao and L. Dong, *J. Colloid Interface Sci.*, 2018, **509**, 334–345.
13 V. P. Pakharukova, E. M. Moroz, V. V. Kriventsov, D. A. Zyuzin, G. R. Kosmambetova and P. E. Strizhak, *Appl. Catal., A*, 2009, **365**, 159–164.
14 Á. Reyes-Carmona, A. Arango-Díaz, E. Moretti, A. Talon, L. Storaro, M. Lenarda, A. Jiménez-López and E. Rodríguez-Castellón, *J. Power Sources*, 2011, **196**, 4382–4387.
15 X. Cheng, L. Wang, Z. Wang, M. Zhang and C. Ma, *Ind. Eng. Chem. Res.*, 2016, **55**, 12710–12722.
16 X. Yao, C. Tang, Z. Ji, Y. Dai, Y. Cao, F. Gao, L. Dong and Y. Chen, *Catal. Sci. Technol.*, 2013, **3**, 688–698.
17 V. D. B. C. Dasireddy and B. Likozar, *Chem. Eng. J.*, 2017, **326**, 886–900.
18 C. A. Sierra-Pereira and E. A. Urquieta-González, *Fuel*, 2014, **118**, 137–147.
19 Z. Gholami and G. Luo, *Ind. Eng. Chem. Res.*, 2018, **57**, 8871–8883.
20 N. F. Sulaiman, W. A. Wan Abu Bakar, S. Toemen, N. M. Kamal and R. Nadarajan, *Renewable Energy*, 2019, **135**, 408–416.
21 H. A. Budiarti, R. N. Puspitasari, A. M. Hatta, S. Koentjoro and D. D. Risanti, *Procedia Eng.*, 2017, **170**, 65–71.
22 M. Zakaulla, A. A. Khan and P. Mukunda, *J. Miner. Mater. Charact. Eng.*, 2014, **2**, 21–25.
23 T. L. Ngai, W. Zheng and Y. Li, *Prog. Nat. Sci.: Mater. Int.*, 2013, **23**, 70–76.
24 M. Konsolakis, G. E. Marnellos, A. Al-Musa, N. Kaklidis, I. Garagounis and V. Kyriakou, *Chin. J. Catal.*, 2015, **36**, 509–516.
25 X. Yao, Y. Xiong, J. Sun, F. Gao, Y. Deng, C. Tang and L. Dong, *J. Rare Earths*, 2014, **32**, 131–138.
26 D. Zhang, L. Zhang, C. Fang, R. Gao, Y. Qian, L. Shi and J. Zhang, *RSC Adv.*, 2013, **3**, 8811–8819.
27 L. Zhou, X. Li, Z. Yao, Z. Chen, M. Hong, R. Zhu, Y. Liang and J. Zhao, *Sci. Rep.*, 2016, **6**, 23900–23906.
28 Y. Gao, K. Xie, W. Wang, S. Mi, N. Liu, G. Pan and W. Huang, *Catal. Sci. Technol.*, 2015, **5**, 1568–1579.
29 Y. Yang, D. Xu, Q. Wu and P. Diao, *Sci. Rep.*, 2016, **6**, 1–13.
30 A. Brenner, *Electrodeposition of Alloys: Principles and Practice*, Elsevier Science, New York, 2013.
31 E. Botcharova, M. Heilmaier, J. Freudenberger, G. Drew, D. Kudashow, U. Martin and L. Schultz, *J. Alloys Compd.*, 2003, **351**, 119–125.
32 K. S. W. Sing and R. T. Williams, *Adsorpt. Sci. Technol.*, 2004, **22**, 773–782.
33 M. Thommes, *Chem. Ing. Tech.*, 2010, **82**, 1059–1073.
34 G. Allaedini, S. M. Tasirin and P. Aminayi, *Chem. Pap.*, 2016, **70**, 231–242.
35 D. Baojuan, L. Shumin, L. Deliang, Z. Ruozhu, L. Jingge, H. Qinglan and B. Feng, *RSC Adv.*, 2016, **6**, 53852–53859.
36 M. Streckova, H. Hadraba, R. Bures, M. Faberova, P. Roupcova, I. Kubena, L. Medvecky, V. Girman, P. Kollar, J. Fuzer and E. Cizmar, *Surf. Coat. Technol.*, 2015, **270**, 66–76.
37 S. Kanungo, K. S. Keshri, E. J. M. Hensen, B. Chowdhury, J. C. Schouten and M. F. Neira d'Angelo, *Catal. Sci. Technol.*, 2018, **8**, 3052–3059.
38 M. L. P. Antunes, N. C. d. Cruz, A. d. O. Delgado, S. F. Durrant, J. R. R. Bortoleto, V. F. Lima, P. L. Santana, L. Caseli and E. C. Rangel, *Mater. Res.*, 2014, **17**, 1316–1323.
39 Y. Zhao, F. Dong, W. Han, H. Zhao and Z. Tang, *RSC Adv.*, 2018, **8**, 1583–1592.
40 S. Lai, D. Meng, W. Zhan, Y. Guo, Y. Guo, Z. Zhang and G. Lu, *RSC Adv.*, 2015, **5**, 90235–90244.
41 D. Meng, W. Zhan, Y. Guo, Y. Guo, L. Wang and G. Lu, *ACS Catal.*, 2015, **5**, 5973–5983.
42 C. Deng, B. Li, L. Dong, F. Zhang, M. Fan, G. Jin, J. Gao, L. Gao, F. Zhang and X. Zhou, *Phys. Chem. Chem. Phys.*, 2015, **17**, 16092–16109.
43 M. S. Shafeeyan, W. M. A. W. Daud, A. Houshmand and A. Shamiri, *J. Anal. Appl. Pyrolysis*, 2010, **89**, 143–151.
44 S.-C. Ma, J.-J. Yao, L. Gao, X.-Y. Ma and Y. Zhao, *J. Air Waste Manage. Assoc.*, 2012, **62**, 1012–1021.
45 X. Yao, Q. Yu, Z. Ji, Y. Lv, Y. Cao, C. Tang, F. Gao, L. Dong and Y. Chen, *Appl. Catal., B*, 2013, **130–131**, 293–304.
46 P. Li, L. Feng, F. Yuan, D. Wang, Y. Dong, X. Niu and Y. Zhu, *Catalysts*, 2016, **6**, 124–142.
47 X. Zhang, S. Cheng, W. Zhang, C. Zhang, N. E. Drewett, X. Wang, D. Wang, S. J. Yoo, J.-G. Kim and W. Zheng, *Ind. Eng. Chem. Res.*, 2017, **56**, 11042–11048.
48 S. Fukuzumi, *ECS J. Solid State Sci. Technol.*, 2017, **6**, M3055–M3061.

49 Z. Bingsen and S. D. Sheng, *ChemCatChem*, 2015, **7**, 3639–3645.
50 A. Martínez-Arias, A. B. Hungría, A. Iglesias-Juez, M. Fernández-García, J. A. Anderson, J. C. Conesa, G. Munuera and J. Soria, *Catal. Today*, 2012, **180**, 81–87.
51 S. D. Senanayake, N. A. Pappoe, T.-D. Nguyen-Phan, S. Luo, Y. Li, W. Xu, Z. Liu, K. Mudiyanselage, A. C. Johnston-Peck, A. I. Frenkel, I. Heckler, D. Stacchiola and J. A. Rodriguez, *Surf. Sci.*, 2016, **652**, 206–212.
52 A. Devadoss, P. Sudhagar, C. Ravidhas, R. Hishinuma, C. Terashima, K. Nakata, T. Kondo, I. Shitanda, M. Yuasa and A. Fujishima, *Phys. Chem. Chem. Phys.*, 2014, **16**, 21237–21242.
53 S. Wu, G. Wen, J. Wang, J. Rong, B. Zong, R. Schlögl and D. S. Su, *Catal. Sci. Technol.*, 2014, **4**, 4183–4187.
54 L. Wang, H. Zhang, G. Cao, W. Zhang, H. Zhao and Y. Yang, *Electrochim. Acta*, 2015, **186**, 654–663.
55 D. Lu, O. A. Zelekew, A. K. Abay, Q. Huang, X. Chen and Y. Zheng, *RSC Adv.*, 2019, **9**, 2018–2025.
56 H. Hernández-Arriaga, E. López-Luna, E. Martínez-Guerra, M. M. Turrubiartes, A. G. Rodríguez and M. A. Vidal, *J. Appl. Phys.*, 2017, **121**, 1–11.
57 K. Safeen, V. Micheli, R. Bartali, G. Gottardi and N. Laidani, *J. Phys. D: Appl. Phys.*, 2015, **48**, 1–13.
58 A. Celebioglu, S. Vempati, C. Ozgit-Akgun, N. Biyikli and T. Uyar, *RSC Adv.*, 2014, **4**, 61698–61705.
59 P. K. Nayak, J. Caraveo-Frescas, Z. Wang, M. N. Hedhili, Q. Wang and H. N. Alshareef, *Sci. Rep.*, 2014, **4**, 1–7.
60 J. Raja, C. P. T. Nguyen, C. Lee, N. Balaji, S. Chatterjee, K. Jang, H. Kim and J. Yi, *IEEE Electron Device Lett.*, 2016, **37**, 1272–1275.
61 Y. Sun, H. Cui, C. Pang and C. Wang, *CrystEngComm*, 2013, **15**, 6477–6482.
62 M. Kamble, V. Waman, A. Mayabadi, S. Ghosh, B. Gabhale, S. Rondiya, A. Rokade, S. Khadtare, V. Sathe and T. Shripathi, *J. Coat.*, 2014, 1–11.
63 F. Deku, S. Mohammed, A. Joshi-Imre, J. Maeng, V. Danda, T. J. Gardner and S. F. Cogan, *J. Biomed. Mater. Res., Part B*, 2019, **107**, 1654–1661.
64 R. Fukuda, S. Sakai, N. Takagi, M. Matsui, M. Ehara, S. Hosokawa, T. Tanaka and S. Sakaki, *Catal. Sci. Technol.*, 2018, **8**, 3833–3845.
65 I. Spassova, M. Khristova, D. Panayotov and D. Mehandjiev, *J. Catal.*, 1999, **185**, 43–57.

